ACS Sustainable Chemistry & Engineering

Research Article

Cite This: ACS Sustainable Chem. Eng. 2019, 7, 8458−8465

pubs.acs.org/journal/ascecg

Supported Heterostructured MoC/Mo_2C Nanoribbons and Nanoflowers as Highly Active Electrocatalysts for Hydrogen Evolution Reaction

Zhaoqian Wei,[†] Xiao Hu,[†] Shunlian Ning,[†] Xiongwu Kang,*[,†] and Shaowei Chen*[,†,‡]

[†]Guangzhou Key Laboratory for Surface Chemistry of Energy Materials, New Energy Research Institute, School of Environment and Energy, South China University of Technology, Higher Education Mega Center, 382 East Waihuan Road, Guangzhou 510006, China

[‡]Department of Chemistry and Biochemistry, University of California, 1156 High Street, Santa Cruz, California 95064, United States

Supporting Information

ABSTRACT: Development of low-cost and high-efficiency electrocatalysts for hydrogen evolution reaction is a critical step toward sustainable water splitting. Herein, in situ growth of heterostructured MoC/Mo_2C nanoribbons and nanoflowers on copper foam (Mo_xC/Cu), copper foil, and nickel foam (Mo_xC/Ni) are prepared via a two-step method: hydrothermal preparation of molybdenum precursors followed by pyrolysis at controlled temperatures. The Mo_xC/Cu hybrids are found to exhibit an excellent catalytic activity, as compared to the Mo_xC/Ni and Cu foil counterparts, and the sample prepared at 750 °C stands out as the best among the series with a low overpotential of 169 mV to reach the current density of 200 mA cm^{-2} in 1 M KOH, and 194 mV in 0.5 M H_2SO_4, and the corresponding Tafel slopes of 98 and 74 mV dec^{-1}, respectively. The electrocatalytic activity is also found to vary with the Mo^{2+}/Mo^{3+} and N contents in the samples that impact the electrical conductivity and electron-transfer kinetics of the hydrogen evolution reaction. Results suggest that MoC/Mo_2C heterostructured materials supported on copper foam may be a viable candidate to catalyze hydrogen evolution reaction in a wide range of pH.

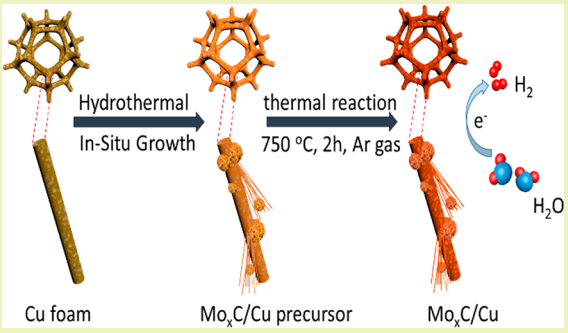

KEYWORDS: *Cu foam, Impedance, N-Doping, Water splitting, Hydrothermal, Interfacial charge transfer, Adsorption, Desorption*

INTRODUCTION

The rapid growth of global energy consumption and related environmental issues have triggered an urgent demand for renewable and clean energy sources.[1,2] As a promising clean and renewable energy carrier, hydrogen has received extensive attention.[3,4] It has been noticed that electrolysis of water is a viable method for the efficient production of hydrogen and can help reduce or even eliminate the requirement for expensive hydrogen transport and distribution infrastructure.[5] Thus, it has been of both fundamental and technological significance to develop low-cost, high-performance electrocatalyst for hydrogen evolution reaction (HER). Molybdenum carbides (e.g., Mo_2C and MoC) have been recognized as a viable candidate due to its low costs and Pt-like d-band electronic structure and HER activity.[6,7] However, in earlier studies, molybdenum carbides are mostly prepared in the powder form[8−12] and involve rather tedious preparation procedures,[13,14] use of expensive organic solvents,[12] and high-temperature annealing, which greatly restrict their commercial utilization.[15] Additionally, the use of a polymer binder to immobilize the catalyst onto a glassy carbon electrode inevitably generates impedance against electron and mass transport and limits the catalytic activity.[16]

Such glued catalysts may also detach from the glassy carbon electrode surface during the electrolysis with a continuing release of hydrogen bubbles, thus compromising the structural integrity and durability of the catalysts.[17−20] Recent studies have shown that three-dimensional (3D) self-supported electrodes on copper foam or nickel foam, such as (i) Cu-encased N-doped carbon nanotube arrays directly grown on copper form,[17] (ii) nickel form-supported $Cu_2O_xS_{1-x}$,[21] Cu_3P/Cu,[22] NiCoP@Cu_3P,[23] Ni_5P_4−Ni_2P,[24] and Ni_2P nanosheets,[25] and (iii) copper form-supported Ni-CeO_2Gd[26] and Cu@NiFe layered double hydroxide,[27] exhibit excellent HER performance, as compared to the planar electrodes. However, the high annealing temperature required for the preparation of Mo_xC and the easy oxidation of the Cu and Ni substrates during the transformation of Mo_xC precursor to Mo_xC result in a loss of their electrical conductivity and HER activity.

Herein, in situ growth of porous Mo_xC on copper foam (Mo_xC/Cu) was prepared by a two-step thermal procedure. The 3D porous and conductive matrices were found to

Received: January 12, 2019
Revised: February 27, 2019
Published: March 31, 2019

DOI: 10.1021/acssuschemeng.9b00210
ACS Sustainable Chem. Eng. 2019, 7, 8458−8465

Scheme 1. Schematic Illustration of the Synthesis of Mo_xC/Cu Nanostructures

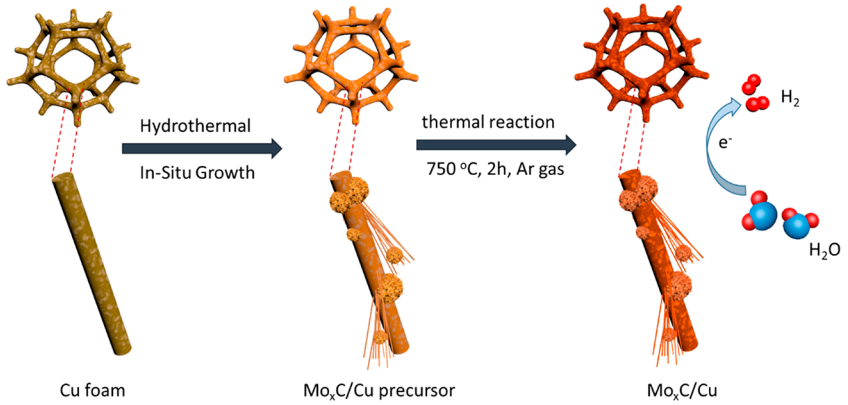

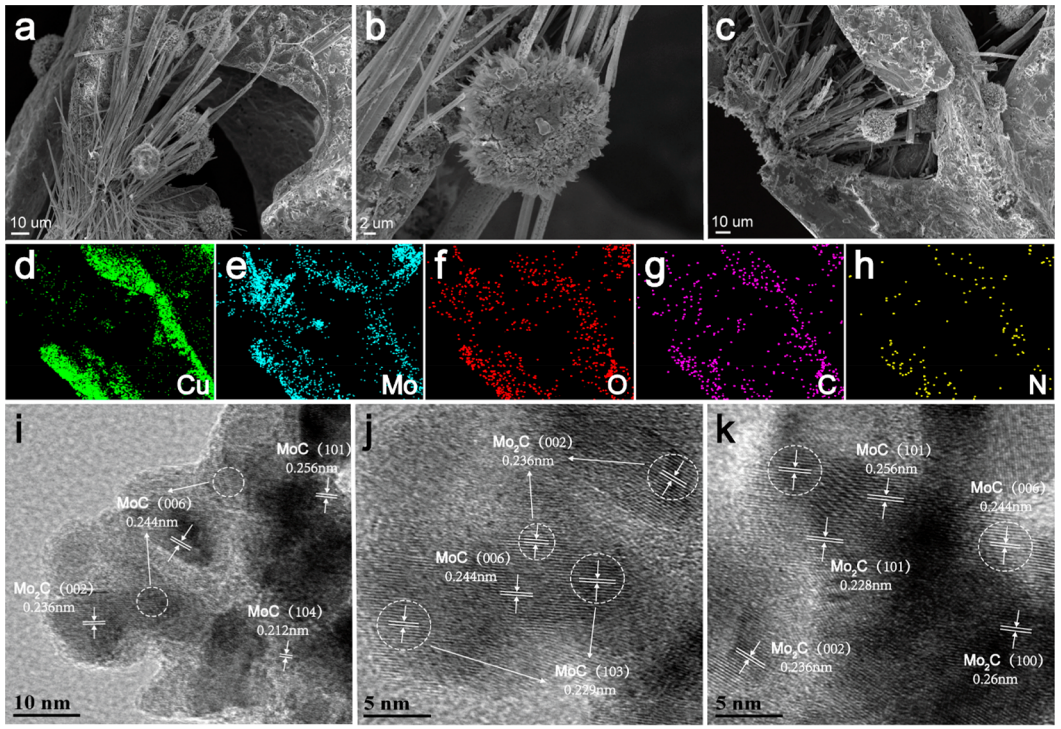

Figure 1. (a–c) SEM images, (d–h) corresponding elemental maps, and (i–k) TEM images of the Mo_xC/Cu-2 sample.

facilitate charge transfer and mass transport (e.g., gas bubble release). In fact, experimental measurements suggest a high and durable activity in both alkaline and acidic media, exhibiting a low overpotential of 169 and 194 mV to reach the current density of 200 mA cm^{-2}, and a Tafel slope of 98 and 74 mV dec^{-1} in 1 M KOH and 0.5 M H_2SO_4, respectively.

EXPERIMENTAL SECTION

Chemicals. Ammonium heptamolybdate tetrahydrate (AHMT, 99.0%, Sinopharm Chemical Reagents), dicyandiamide (DCDA, Johnson Matthey Corporation), and Pt/C (20 wt % Pt on Vulcan XC72R, Johnson Matthey Corporation) were used as received. Copper and nickel foams (thickness ~1.6 mm, Suzhou Taili Co.) were polished before use. Deionized water was purified using a Milli-Q system (18.2 MΩ cm, Millipore, Billerica, U.S.A.).

Synthesis of N-Doped Mo_xC/Cu. To achieve robust contact between Mo_xC and the substrate and thus assuring enhanced interfacial charge transfer, Mo_xC/Cu was prepared by in situ growth by following a two-step method,[28] as shown in Scheme 1. First, a copper foam (4 cm × 2 cm) was sonicated in diluted hydrochloric acid (~2 M), deionized water, and ethanol sequentially to remove oxides and organic contaminants on the surface. Mo_xC/Cu precursor was then prepared by following a prior procedure,[28] where 1.74 g of AHMT was dissolved in 70 mL of deionized water (20 mM) at room temperature and transferred into a Teflon-lined stainless-steel autoclave (100 mL). The copper foam was then submerged upright into the solution in the autoclave. The autoclave was sealed and heated at 100 °C for 18 h in an oven. After naturally cooling down to room temperature, the resulting copper foam was washed with deionized water and ethanol several times and then dried at 60 °C in a vacuum oven overnight.

The precursor obtained above was placed at the center of a tube furnace, and a calculated amount of DCDA was put at the upstream of the precursor, which were annealed at 450 °C for 2 h and then at 650, 750, or 850 °C for another 2 h under an Ar atmosphere, at the heating rate of 5 °C min^{-1}. The obtained samples were denoted as Mo_xC/Cu-1, Mo_xC/Cu-2, and Mo_xC/Cu-3, respectively. The heterostructured Mo_xC supported on copper foil or Ni foam was prepared by following the same procedure except that a nickel foam was used instead of a copper foam.

DOI: 10.1021/acssuschemeng.9b00210
ACS Sustainable Chem. Eng. 2019, 7, 8458–8465

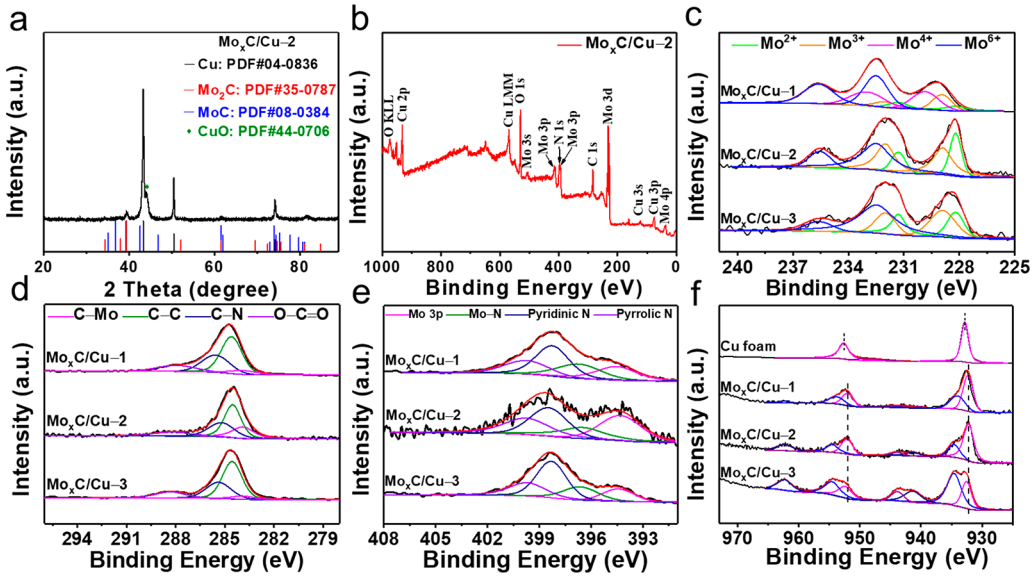

Figure 2. (a) XRD patterns and (b) XPS survey spectrum of Mo$_x$C/Cu-2. High-resolution XPS spectra of the (c) Mo 3d, (d) C 1s, (e) N 1s, and (f) Cu 2p electrons of the Mo$_x$C/Cu-*n* samples (*n* = 1, 2, and 3).

Synthesis of Pt/C/Cu. To prepare Pt/C catalytic electrode, 10 mg Pt/C and 50 μL of 5 wt % Nafion solution was evenly dispersed in water/ethanol mixed solution (500 μL of ultrapure water and 450 μL of ethanol) by ultrasonication for 30 min. An appropriate amount of the catalyst ink was uniformly dropped onto the copper foam and dried in the air.

Characterizations. Powder X-ray diffraction (XRD) patterns was recorded with a Bruker D8 Advance powder X-ray diffractometer with Cu Kα (λ = 0.15406 nm) radiation. X-ray photoelectron spectroscopic (XPS) measurements were performed using a PHI X-tool instrument (Ulvac-Phi). Raman spectra were acquired with a Horiba LabRAM HR Evolution system equipped with a semiconductor laser (λ = 532 nm, Laser Quantum Ltd). The morphology of the samples and elemental mapping analysis was carried out with a Hitachi S-4800 field-emission scanning electron microscope (SEM) based on energy-dispersive X-ray spectroscopy (EDS). High-resolution transmission electron microscopy (HRTEM) studies were performed with a JEOL TEM-2010 instrument.

Electrochemistry. Electrochemical characterization was conducted in a three-electrode configuration with a CHI 650E electrochemical station in 1.0 M KOH or 0.5 M H_2SO_4 at room temperature. A saturated calomel electrode (SCE, in saturated KCl) and a graphite rod were used as the reference and counter electrode, respectively. The SCE was calibrated with respect to a reversible hydrogen electrode (RHE), and all potentials in the present study were referenced to the RHE. The obtained Mo$_x$C/Cu was cut into small pieces of around 0.5 cm × 1.0 cm and used directly as the working electrode. Polarization curves were acquired by sweeping the potential from 0 to −0.5 V (vs RHE) in 1.0 M KOH and 0.5 M H_2SO_4 at the potential sweep rate of 5 mV s^{-1}. The current density (j) was calculated based on the geometric area of the electrode, and the polarization curves were collected with *i*R compensation. Cyclic voltammetry (CV) was used to probe the electrochemical double layer capacitance in a non-Faradaic region at different scan rates as a means to estimate the effective electrode surface area. Electrochemical impedance spectroscopy (EIS) was carried out with an AC amplitude of 5 mV in the frequency range of 100 kHz to 0.01 Hz. The main arc in each EIS spectrum was fitted by using a simplified Randles equivalent circuit, which was comprised of a resistance (R_s) in series with a parallel arrangement of a charge-transfer resistance (R_{ct}) and a constant phase element (CPE).

RESULTS AND DISCUSSION

Structural Characterization. From the SEM images in Figure S1–S2, one can see that hydrothermal treatment of ammonium heptamolybdate tetrahydrate led to the grown of abundant nanoribbons and nanoflowers on the copper foam surface. Such structural morphologies were retained after calcination of the obtained precursor in the presence of DCDA, as exemplified by Mo$_x$C/Cu-2 that were prepared at 750 °C (Figure 1a–c). EDS-based element mapping analysis (Figure 1d-h) shows rather homogeneous distributions of the Mo, O, C, and N elements throughout the observed area. Consistent results were obtained with the Mo$_x$C/Ni samples (Figures S3 and S4a–c).

The corresponding TEM images of Mo$_x$C/Cu-2 are shown in Figures S5 and Figure 1i–k, where nanoparticles of ca. 20 nm in diameter can be clearly observed and exhibit well-defined lattice fringes. As illustrated in Figure 1i–k, the interplanar spacings of 0.256 nm, 0.244 nm, 0.229 and 0.212 nm are consistent with the (101), (006), (103), and (104) facets of MoC (JCPDS no. 08–0384), while the lattice spacings of 0.236, 0.228, and 0.260 nm can be indexed to the (002), (101), and (100) facets of Mo_2C (JCPDS no. 35–0787).[29] These results suggest the formation of MoC and Mo_2C heterostructures in the sample.

Further structural insights were obtained by XRD and XPS measurements. Figure 2a depicts the XRD patterns of the Mo$_x$C/Cu-2 sample, where three major peaks can be identified at 43.3°, 50.4°, and 74.1° that arose from the (111), (200), and (220) diffractions of the copper foam (black line, JCPDS No. 04–0836), along with another one at 44.2° for CuO (green quadrilateral, JCPDS No. 44-0706). Four additional diffraction peaks can be seen at 34.4°, 39.3°, 61.5°, and 81.2° that can be assigned to the (100), (110), (103), and (004) diffractions of Mo$_x$C species (Mo_2C: red line, JCPDS no. 35-0787; MoC: blue line, JCPDS no. 08-0384). Note that the XRD patterns of the precursor sample (Figure S6a) are completely different from those of Mo$_x$C/Cu, suggesting complete conversion of the precursor to Mo$_x$C by pyrolysis at elevated temperatures. Similar behaviors were observed with the Mo$_x$C/Ni sample,

DOI: 10.1021/acssuschemeng.9b00210
ACS Sustainable Chem. Eng. 2019, 7, 8458–8465

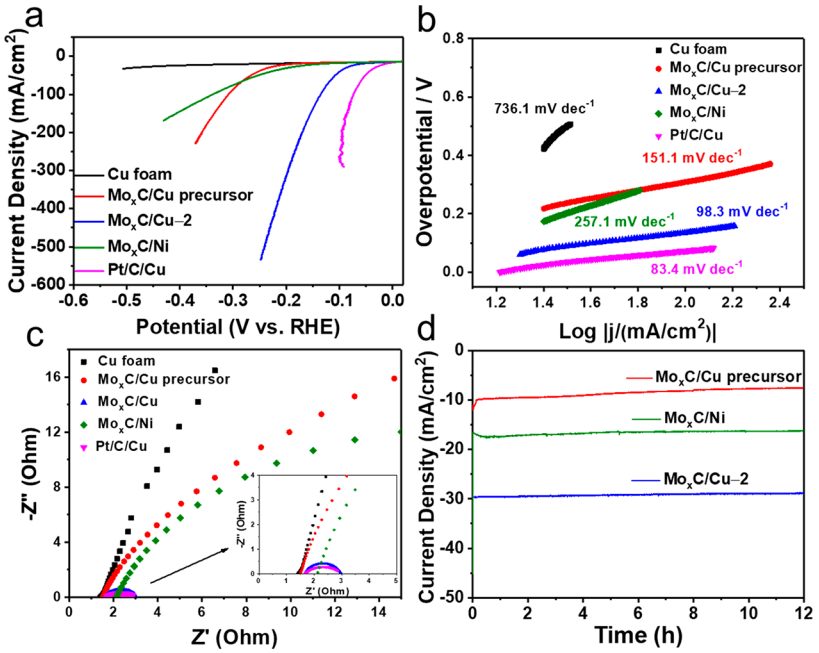

Figure 3. (a) LSV polarization curves, (b) Tafel plots, and (c) Nyquist plots at the overpotential of 132 mV with the Cu foam, Pt/C, Mo_xC/Cu precursor, Mo_xC/Cu-2, and Mo_xC/Ni electrodes. (d) HER stability test of Mo_xC/Cu precursor, Mo_xC/Ni, and Mo_xC/Cu-2 at a static overpotential of 82.5 mV. All experiments were carried out in 1 M KOH.

except that the nickel foam exhibited three major diffraction peaks at 44.5°, 51.8°, and 76.4° (black line, JCPDS No. 04-0836; Figure S7).

XPS studies were then carried out to analyze the elemental composition and valence states of the samples. Although the exact content of Mo_xC/Cu precursor cannot be indentified by XRD (Figure S6a), Mo $3d_{5/2}$ and $3d_{3/2}$ was at 232.5 and 235.6 eV, which is accounted for the molybdate (Mo^{6+}; Figure S6c). From the full survey spectra of Mo_xC/Cu-2 (Figure 2b) and its precursor (Figure S6b), the Mo, Cu, C, N, and O elements are clearly observed. Figure 2c–f show the high-resolution XPS spectra of Mo, C, N, and Cu for Mo_xC/Cu-*n* (*n* = 1, 2, and 3). For Mo_xC/Cu-1 prepared at 650 °C, the Mo spectrum can be deconvoluted into four pairs of subpeaks at (228.2, 231.3 eV), (228.9, 232.0 eV), (229.9, 233 eV), and (232.5, 235.6 eV) for the $3d_{5/2}$ and $3d_{3/2}$ electrons of Mo^{2+}, Mo^{3+}, Mo^{4+}, and Mo^{6+}, respectively.[30,31] The presence of Mo^{4+} and Mo^{6+} are usually ascribed to MoO_2 and MoO_3 likely because the sample was exposed to air,[9,32] whereas the Mo^{2+} and Mo^{3+} species are consistent with the formation of Mo_2C and MoC.[33] Furthermore, the atomic ratio of Mo^{3+}/Mo^{2+} and the total contents Mo^{3+} and Mo^{2+} of all Mo species was evaluated for the Mo_xC/Cu series and listed in Table S1. One can see that the atomic ratio and percentage of Mo^{3+}/Mo^{2+} in Mo_xC/Cu-1 is 1.47 and 22.8%. When the pyrolysis temperature was increased to 750 and 850 °C, Mo^{4+} species vanished and the atomic percentage of Mo^{3+}/Mo^{2+} increased to 60.3% and 56.8% for Mo_xC/Cu-2 and Mo_xC/Cu-3, respectively. That is, the Mo_xC/Cu-2 sample shows the highest contents of Mo^{3+}/Mo^{2+}. It has been reported that the Mo^{2+} and Mo^{3+} species are the HER active centers and the variation of the molar ratio of Mo^{3+}/Mo^{2+} is strongly correlated with the electronic density of Mo^{3+} and Mo^{2+} and hence the HER activity.[8,10] Therefore, the formation of MoC/Mo_2C heterostructures may improve the HER activity by mediating the hydrogen adsorption energy at the MoC/Mo_2C interface (vide infra).[34,35]

In Figure 2d, the C 1s XPS spectra of the Mo_xC/Cu samples are deconvoluted into four peaks at 283.8, 284.5, 285.2, and 288.3 eV, which correspond to C–Mo, C–C, C–N, and O–C=O, respectively.[36,37] The presence of C–Mo at 283.8 eV further supports the formation of Mo_xC heterostructures on Cu foam and the C–N at 285.2 eV indicate the successful doping of N into the carbon layer, which may promote the electronic conductivity of carbon matrix.[38] The largest content of Mo–C is 20.7% in Mo_xC-2, corresponding to the largest content of Mo_xC. Note that the N-dopants and Mo_xC behave as electron acceptors and donors respectively for the adjacent C atoms in the carbon materials, producing highly active carbon active sites in carbon materials.[14,39]

Figure 2e shows the high-resolution XPS spectra of the N 1s electrons. Deconvolution yielded four subpeaks at 394.3, 396.5, 398.5, and 399.8 eV, which can be assigned to Mo 3p, Mo–N, pyridinic–N, and pyrrolic–N, respectively.[31,40−42] The Mo–N at 396.5 eV confirms N doping in Mo_xC/Cu, which was the highest at 23.2 at. % with Mo_xC/Cu-2, in comparison to 18.7 at. % for Mo_xC/Cu-1 and 15.5 at. % for Mo_xC/Cu-3. These N-dopants may also enhance the local concentration of protons near the catalyst surface and promote the HER activity.[43] The lower N doping in Mo_xC/Cu-1 may be caused by inadequate calcination while that for Mo_xC/Cu-3 was likely due to the decomposition of unstable N dopants at high temperatures.[44,45] In Raman measurements, the Mo_xC/Cu samples (Figure S6f) all exhibited two characteristic peaks at ca. 1355 and 1575 cm^{-1}, due to the D and G bands of graphitic carbon, suggesting that Mo_xC/Cu were indeed imbedded in a carbon matrix.[11,44] By contrast, no graphitic C was observed with the precursor on the Cu foam.

The high-resolution XPS spectra of the Cu 2p electrons are shown in Figure 2f. The Cu $2p_{3/2}$ and Cu $2p_{1/2}$ binding energies can be observed at 932.8 and 952.7 eV for the pristine Cu foam, and somewhat negatively shifted to 932.2 and 952.1 eV for Mo_xC/Cu-2 (Table S2), suggesting charge transfer from

DOI: 10.1021/acssuschemeng.9b00210
ACS Sustainable Chem. Eng. 2019, 7, 8458−8465

Mo_xC to Cu substrate since the work function of the former is lower than the latter (4.5 eV vs 3.4 eV).[45] The shakeup Cu satellite at 941.4, 943.9, and 962.3 eV observed with the Mo_xC/Cu series indicate oxidized copper species.[46−48] The subpeaks for oxidized Cu $2p_{3/2}$ and $2p_{1/2}$ were observed at 933.8 and 953.7 eV for the precursor and Mo_xC/Cu-1, and apparently positively shifted to 934.6 and 954.5 eV for Mo_xC/Cu-2 and Mo_xC/Cu-3. However, the signal of CuO overwhelmed that of Cu in Mo_xC/Cu-3, possibly because of deep oxidation of copper at high temperatures. This may impede charge transfer between the substrate and Mo_xC and compromise the HER performance (vide infra). Similar behaviors were observed with the Mo_xC/Ni sample and its precursor (Figure S8).

Electrocatalytic Characterization. The HER performance of the series of Mo_xC/Cu-n samples prepared at different temperatures were first characterized in an alkaline electrolyte (Figure S9a-b) and the electrochemical surface area of the Mo_xC/Cu samples was estimated by the double-layer capacitance (Figure S9c).[49,50] One can see that Mo_xC/Cu-2 exhibited the largest electrochemical surface area and best HER activity among the series. The Tafel slopes[51,52] of the Mo_xC/Cu samples were all close to 98 mV dec^{-1}, indicating that HER on Mo_xC/Cu-n most likely followed the Volmer−Heyrovsky mechanism in alkaline media, and the rate−determining step was the electrochemical desorption of H_2. Additionally, the exchange current density (j_0) of Mo_xC/Cu-*n* was estimated by extrapolation of the Tafel plots to the *x*-axis. Mo_xC/Cu-2 exhibited the highest j_0, which might be ascribed to the lowest interfacial charge transfer resistance (R_{ct}) that is almost 1 order of magnitude lower than those of the other two samples (Figure S9d). This is likely due to the highest N dopant, atomic percentage of Mo^{3+}/Mo^{2+} and minimum amount of CuO in Mo_xC/Cu-2 (Tables S1−S2 and Figure S10a-b).[53] As discussed above, the doping of N atoms into the carbon matrix and Mo_xC not only increases the electron density of the surface carbon layers and local concentration of protons[8,13,54−56] but also creates highly active sites on the carbon surface,[39,43] thus enhancing the catalytic performance of HER.

The LSV polarization curves of Mo_xC/Cu-2, bare Cu foam, Mo_xC/Cu precursor, Mo_xC/Ni, and Pt/C/Cu are shown in Figure 3a. The overpotentials needed to reach the current density of 100 and 200 mA cm^{-2} were estimated to be 136 and 169 mV for Mo_xC/Cu-2, respectively, which are markedly lower than those for the precursor (308 and 360 mV) and Mo_xC/Ni (338 mV at 100 mA cm^{-2}), but remained subpar as compared to that of Pt/C (73 mV and 96 mV). Since Mo_2C shows a strong adsorption to H ions that is beneficial to H^+ reduction but hinders H_{ads} desorption, while MoC works in the a opposite way.[57] Thus, the heterostructured MoC/Mo_2C can synergistically regulate both the adsorption and desorption of H^+ and H, thus achieving much enhanced HER activity. The corresponding Tafel plots are shown in Figure 3b. The Tafel slope of Mo_xC/Cu-2 (98 mV dec^{-1}) is comparable to that of Pt/C (83 mV dec^{-1}) but much smaller than those of Mo_xC/Ni (257 mV dec^{-1}) and Mo_xC/Cu precursor (151 mV dec^{-1}), suggesting excellent HER activity of Mo_xC/Cu-2. In addition, the remarkably reduced slope for Mo_xC/Cu-2 confirmed the improved HER kinetics of water splitting. It is worth noting that the HER performance of Mo_xC/Cu-2 is comparable or even better than relevant HER catalysts reported in recent literature (Table S3).

Figure 3c shows the Nyquist plots of Cu foam, Mo_xC/Cu precursor, Mo_xC/Cu, Mo_xC/Ni, and Pt/C acquired at the overpotential of 132 mV. It can be seen that R_{ct} of Mo_xC/Cu-2 is rather comparable to that of Pt/C but significantly smaller than those of Mo_xC/Ni, Mo_xC/Cu precursor, and copper foam, indicating that Mo_xC/Cu-2 possessed a more desirable structures for the electron-transfer kinetics of HER.[58] It should be noted that the interfacial charge transfer resistance of Mo_xC/Ni is about 11 times higher than that of Mo_xC/Cu-2. The extremely slower interfacial charge transfer, as well as the much lower atomic ratio and percentage of Mo^{3+}/Mo^{2+} in Mo_xC/Ni is 0.88 and 37.7% than Mo_xC/Cu-2 (1.78, 60.3%) might account for the poorer HER activity for Mo_xC/Ni than Mo_xC/Cu-2. Additionally, from the Nyquist plots in Figure S11a, R_{ct} of Mo_xC/Cu-2 can be seen to diminish considerably with increasing overpotentials, signifying enhanced electron-transfer kinetics.[28] The Mo_xC/Cu-2 sample also shows a smaller series resistance (R_s), because Mo_xC was formed via direct reactions with the Cu foam, leading to stronger adhesion and better electrical contacts with the substrate.[27]

As shown in Figure S11b-d, the C_{dl} of Mo_xC/Cu-2 (23.4 mF cm^{-2}) was much higher than that of copper foam (1.6 mF cm^{-2}), the precursor (5.5 mF cm^{-2}) and Mo_xC/Ni (4.7 mF cm^{-2}), indicating a much larger active surface area and more exposed active sites on Mo_xC/Cu-2.[59] Mo_xC/Cu-2 also exhibited excellent stability for HER, as shown in Figure 3d. The current density of Mo_xC/Cu-2 at the overpotential of 127 mV remained largely unchanged over a 12 h period. The polarization curves of the Mo_xC/Cu-2 before and after the *i-t* test are characterized (Figure S12). After the *i-t* test, the overpotential at the current density of 100 and 200 mA cm^{-2} was increased by only 7 and 13 mV, respectively, suggesting the excellent electrochemical durability toward HER in 1 M KOH.[57] Figure S13 shows that the morphology of the nanoribbons and nanoflowers of Mo_xC/Cu-2 are well maintained after the *i-t* measurement, further indicating good stability of Mo_xC grown on copper foam. Nevertheless, the precursor and Mo_xC/Ni peeled off from the foam substrate and the current density diminished markedly. Consistent behaviors are observed in acidic media (Figure S14−16), where the Mo_xC/Cu-2 sample exhibits an excellent catalytic activity with an overpotential of 194 mV to reach the current density of 200 mA cm^{-2} in 0.5 M H_2SO_4, and the corresponding Tafel slope is determined to be 74 mV dec^{-1}.

To investigate the impact of the high surface area of copper foam, the Mo_xC was also prepared on the copper foil by the same method and the HER performance in 1 M KOH was shown in Figure S17. The overpotential to achieve 10 mA cm^{-2} for Mo_xC prepared at 650, 750, and 850 °C is 305, 379, and 395 mV, much larger than the counterparts on Cu foam, which is only 232, 80, and 168 mV respectively. In addition, the impedance of Mo_xC on copper foil (Figure S17b) is much larger than that on copper foam. The double layer capacitance of Mo_xC (Figure S17c) on copper foam is approximately 10 times of that on copper foil. The polarization curves are further normalized to ECSA derived from double layer capacitance (Figure S18), and the overpotentials to reach the current density of 0.5 mA cm^{-2} were estimated to be 322.3, 199.8, and 281.4 mV for Mo_xC/Cu-1, Mo_xC/Cu-2, and Mo_xC/Cu-3, respectively, which are markedly lower than that the counterpart on Cu foil (437.5, 424.5, and 422.3 mV) and Ni foam. The superior intrinsic catalytic performance of Mo_xC on Cu foam than that on Cu foil is possibly ascribed to the large

DOI: 10.1021/acssuschemeng.9b00210
ACS Sustainable Chem. Eng. 2019, 7, 8458−8465

contact area between the Cu substrate and the Mo_xC, which is beneficial to the interfacial charge transfer between the Mo_xC and Cu substrate. As demonstrated by the EIS spectra in Figures S9d and S18, the interfacial charge transfer resistance of Mo_xC/Cu-2 is ~27 times lower than the counterpart on Cu foil, in agreement with our anticipation. In addition, the porous structure of Cu foam may also benefit to the mass diffusion from electrolyte to the catalyst surface, further promoting the HER performance.

CONCLUSIONS

In this work, Mo_xC nanoribbons and nanoflowers supported on both copper (Mo_xC/Cu), Cu foil, and nickel foam (Mo_xC/Ni) were prepared by a two-step procedure that entailed hydrothermal growth of the precursors on the metal foam, followed by pyrolytic conversion Mo_xC in the presence of dicyanodiamine. Electron microscopic and spectroscopic measurements confirmed the formation of MoC/Mo_2C heterostructures within the samples. Mo_xC/Cu exhibited an apparent HER activity with a relatively Tafel slope and long-term stability in both alkaline and acid media, and the sample prepared at 750 °C stood out as the best among the series. The excellent performance was ascribed to the 3D porous copper foam substrate that facilitated facile electron/mass transfer and hydrogen release, the high contents of Mo^{2+}/Mo^{3+}, and N dopants that enhanced HER charge-transfer kinetics. Results from this study suggest that Mo_xC heterostructures supported on copper foam can be exploited as effective electrocatalysts toward HER.

ASSOCIATED CONTENT

Supporting Information

The Supporting Information is available free of charge on the ACS Publications website at DOI: 10.1021/acssuschemeng.9b00210.

SEM, TEM, XRD, XPS, Raman, and elemental mapping for Mo_xC/Cu, Mo_xC/Ni, and their precursors; electrochemical performance of Mo_xC/Cu in 1 M KOH and 0.5 M H_2SO_4; determination of electrochemical surface area through double layer capacitance for Cu foam, Mo_xC/Cu precursor, Mo_xC/Cu, and Mo_xC/Ni (PDF)

AUTHOR INFORMATION

Corresponding Authors

*E-mail: esxkang@scut.edu.cn.
*E-mail: shaowei@ucsc.edu.

ORCID

Xiongwu Kang: 0000-0003-2587-4962
Shaowei Chen: 0000-0002-3668-8551

Notes

The authors declare no competing financial interest.

ACKNOWLEDGMENTS

This work was supported by the National Natural Science Foundation of China (No. 51602106) and Guangdong Innovative and Entrepreneurial Research Team Program (No. 2016ZT06N569).

REFERENCES

(1) Dresselhaus, M. S.; Thomas, I. L. Alternative energy technologies. *Nature* **2001**, *414* (6861), 332–7.
(2) Gray, H. B. Powering the planet with solar fuel. *Nat. Chem.* **2009**, *1*, 112.
(3) Chang, Y. H.; Lin, C. T.; Chen, T. Y.; Hsu, C. L.; Lee, Y. H.; Zhang, W.; Wei, K. H.; Li, L. J. Highly efficient electrocatalytic hydrogen production by MoS_x grown on graphene-protected 3D Ni foams. *Adv. Mater.* **2013**, *25* (5), 756–60.
(4) Lubitz, W.; Tumas, W. Hydrogen: an overview. *Chem. Rev.* **2007**, *107* (10), 3900–3.
(5) Wang, H. T.; Lee, H. W.; Deng, Y.; Lu, Z. Y.; Hsu, P. C.; Liu, Y. Y.; Lin, D. C.; Cui, Y. Bifunctional non-noble metal oxide nanoparticle electrocatalysts through lithium-induced conversion for overall water splitting. *Nat. Commun.* **2015**, *6*, 7261.
(6) Zheng, W.; Cotter, T. P.; Kaghazchi, P.; Jacob, T.; Frank, B.; Schlichte, K.; Zhang, W.; Su, D. S.; Schuth, F.; Schlogl, R. Experimental and theoretical investigation of molybdenum carbide and nitride as catalysts for ammonia decomposition. *J. Am. Chem. Soc.* **2013**, *135* (9), 3458–64.
(7) Wan, C.; Regmi, Y. N.; Leonard, B. M. Multiple phases of molybdenum carbide as electrocatalysts for the hydrogen evolution reaction. *Angew. Chem., Int. Ed.* **2014**, *53* (25), 6407–10.
(8) Das, D.; Santra, S.; Nanda, K. K. In situ fabrication of a Nickel/Molybdenum carbide-anchored N-doped Graphene/CNT hybrid: an efficient (Pre)catalyst for OER and HER. *ACS Appl. Mater. Interfaces* **2018**, *10* (41), 35025–35038.
(9) He, C. Y.; Tao, J. Z. Exploration of the electrochemical mechanism of ultrasmall multiple phases molybdenum carbides nanocrystals for hydrogen evolution reaction. *RSC Adv.* **2016**, *6* (11), 9240–9246.
(10) Xu, G.-R.; Bai, J.; Yao, L.; Xue, Q.; Jiang, J.-X.; Zeng, J.-H.; Chen, Y.; Lee, J.-M. Polyallylamine-functionalized platinum tripods: Enhancement of hydrogen evolution reaction by proton carriers. *ACS Catal.* **2017**, *7* (1), 452–458.
(11) Lv, C. C.; Huang, Z. P.; Yang, Q. P.; Zhang, C. Nanocomposite of MoO_2 and MoC loaded on porous carbon as an efficient electrocatalyst for hydrogen evolution reaction. *Inorg. Chem. Front.* **2018**, *5* (2), 446–453.
(12) Shi, Z.; Gao, B.; Mo, Q.; Shao, Z.-J.; Nie, K.; Liu, B.; Zhang, H.; Wang, Y.; Zhang, Y.; Gao, Q.; Sun, X.; Cao, X.-M.; Hu, P.; Tang, Y. Organic–inorganic-hybrid-derived molybdenum carbide nanoladders: Impacts of surface oxidation for hydrogen evolution reaction. *ChemNanoMat* **2018**, *4* (2), 194–202.
(13) Jiang, R.; Fan, J. H.; Hu, L. Y.; Dou, Y. P.; Mao, X. H.; Wang, D. H. Electrochemically synthesized N-doped molybdenum carbide nanoparticles for efficient catalysis of hydrogen evolution reaction. *Electrochim. Acta* **2018**, *261*, 578–587.
(14) Li, J.; Zhou, C. M.; Mu, J. S.; Yang, E. C.; Zhao, X. J. In situ synthesis of molybdenum carbide/N-doped carbon hybrids as an efficient hydrogen-evolution electrocatalyst. *RSC Adv.* **2018**, *8* (31), 17202–17208.
(15) Gao, M. Y.; Yang, C.; Zhang, Q. B.; Zeng, J. R.; Li, X. T.; Hua, Y. X.; Xu, C. Y.; Dong, P. Facile electrochemical preparation of self-supported porous Ni–Mo alloy microsphere films as efficient bifunctional electrocatalysts for water splitting. *J. Mater. Chem. A* **2017**, *5* (12), 5797–5805.
(16) Wang, J.; Zhong, H. X.; Wang, Z. L.; Meng, F. L.; Zhang, X. B. Integrated three-dimensional carbon paper/carbon tubes/cobalt-sulfide sheets as an efficient electrode for overall water splitting. *ACS Nano* **2016**, *10* (2), 2342–8.
(17) Zhang, Y.; Ma, Y.; Chen, Y. Y.; Zhao, L.; Huang, L. B.; Luo, H.; Jiang, W. J.; Zhang, X.; Niu, S.; Gao, D.; Bi, J.; Fan, G.; Hu, J. S. Encased copper boosts the electrocatalytic activity of N-doped carbon nanotubes for hydrogen evolution. *ACS Appl. Mater. Interfaces* **2017**, *9* (42), 36857–36864.
(18) Zhang, X.; Liu, R.; Zang, Y.; Liu, G.; Wang, G.; Zhang, Y.; Zhang, H.; Zhao, H. Co/CoO nanoparticles immobilized on Co-N-doped carbon as trifunctional electrocatalysts for oxygen reduction, oxygen evolution and hydrogen evolution reactions. *Chem. Commun.* **2016**, *52* (35), 5946–9.

(19) Roy-Mayhew, J. D.; Boschloo, G.; Hagfeldt, A.; Aksay, I. A. Functionalized graphene sheets as a versatile replacement for platinum in dye-sensitized solar cells. *ACS Appl. Mater. Interfaces* **2012**, *4* (5), 2794−800.
(20) Luo, Y. S.; Jiang, J.; Zhou, W. W.; Yang, H. P.; Luo, J. S.; Qi, X. Y.; Zhang, H.; Yu, D. Y. W.; Li, C. M.; Yu, T. Self-assembly of well-ordered whisker-like manganese oxide arrays on carbon fiber paper and its application as electrode material for supercapacitors. *J. Mater. Chem.* **2012**, *22* (17), 8634−8640.
(21) Zhang, X.; Cui, X.; Sun, Y.; Qi, K.; Jin, Z.; Wei, S.; Li, W.; Zhang, L.; Zheng, W. Nanoporous sulfur-doped copper oxide ($Cu_2O_xS_{1-X}$) for overall water splitting. *ACS Appl. Mater. Interfaces* **2018**, *10* (1), 745−752.
(22) Lu, C.; Wang, J. Y.; Czioska, S.; Dong, H.; Chen, Z. F. Hierarchically structured Cu-based electrocatalysts with nanowires array for water splitting. *J. Phys. Chem. C* **2017**, *121* (46), 25875−25881.
(23) Ma, X. X.; Chang, Y. Q.; Zhang, Z.; Tang, J. L. Forest-like NiCoP@Cu_3P supported on copper foam as a bifunctional catalyst for efficient water splitting. *J. Mater. Chem. A* **2018**, *6* (5), 2100−2106.
(24) Wang, X.; Kolen'ko, Y. V.; Bao, X. Q.; Kovnir, K.; Liu, L. One-step synthesis of self-supported nickel phosphide nanosheet array cathodes for efficient electrocatalytic hydrogen generation. *Angew. Chem., Int. Ed.* **2015**, *54* (28), 8188−92.
(25) Shi, Y.; Xu, Y.; Zhuo, S.; Zhang, J.; Zhang, B. Ni_2P Nanosheets/Ni Foam Composite Electrode for Long-Lived and pH-Tolerable Electrochemical Hydrogen Generation. *ACS Appl. Mater. Interfaces* **2015**, *7* (4), 2376−84.
(26) Sivasakthi, P.; Premlatha, S.; Bapu, G. N. K. R.; Chandrasekaran, M. Pulse electrodeposited Ni-CeO_2Gd doped nanocomposite on copper foam as an electrocatalysts for hydrogen evolution reaction. *Int. J. Hydrogen Energy* **2017**, *42* (8), 4741−4750.
(27) Yu, L.; Zhou, H. Q.; Sun, J. Y.; Qin, F.; Yu, F.; Bao, J. M.; Yu, Y.; Chen, S.; Ren, Z. F. Cu nanowires shelled with NiFe layered double hydroxide nanosheets as bifunctional electrocatalysts for overall water splitting. *Energy Environ. Sci.* **2017**, *10* (8), 1820−1827.
(28) Du, C. C.; Shang, M. X.; Mao, J. X.; Song, W. B. Hierarchical MoP/Ni_2P heterostructures on nickel foam for efficient water splitting. *J. Mater. Chem. A* **2017**, *5* (30), 15940−15949.
(29) Wang, D. Z.; Guo, T.; Wu, Z. Z. Hierarchical Mo_2C/C scaffolds organized by nanosheets as highly efficient electrocatalysts for hydrogen production. *ACS Sustainable Chem. Eng.* **2018**, *6* (11), 13995−14003.
(30) Zhao, Y.; Kamiya, K.; Hashimoto, K.; Nakanishi, S. In situ CO_2-emission assisted synthesis of molybdenum carbonitride nanomaterial as hydrogen evolution electrocatalyst. *J. Am. Chem. Soc.* **2015**, *137* (1), 110−3.
(31) Ma, R.; Zhou, Y.; Chen, Y.; Li, P.; Liu, Q.; Wang, J. Ultrafine molybdenum carbide nanoparticles composited with carbon as a highly active hydrogen-evolution electrocatalyst. *Angew. Chem., Int. Ed.* **2015**, *54* (49), 14723−7.
(32) Guo, J. P.; Wang, J.; Wu, Z. X.; Lei, W.; Zhu, J.; Xia, K. D.; Wang, D. L. Controllable synthesis of molybdenum-based electrocatalysts for a hydrogen evolution reaction. *J. Mater. Chem. A* **2017**, *5* (10), 4879−4885.
(33) Lin, H.; Shi, Z.; He, S.; Yu, X.; Wang, S.; Gao, Q.; Tang, Y. Heteronanowires of MoC-Mo_2C as efficient electrocatalysts for hydrogen evolution reaction. *Chem. Sci.* **2016**, *7* (5), 3399−3405.
(34) Kou, Z.; Wang, T.; Cai, Y.; Guan, C.; Pu, Z.; Zhu, C.; Hu, Y.; Elshahawy, A. M.; Wang, J.; Mu, S. Ultrafine molybdenum carbide nanocrystals confined in carbon foams via a colloid-confinement route for efficient hydrogen production. *Small Methods* **2018**, *2* (4), 1700396.
(35) Ji, L.; Wang, J.; Teng, X.; Dong, H.; He, X.; Chen, Z. N,P-doped molybdenum carbide nanofibers for efficient hydrogen production. *ACS Appl. Mater. Interfaces* **2018**, *10* (17), 14632−14640.
(36) Pu, Z.; Amiinu, I. S.; Zhang, C.; Wang, M.; Kou, Z.; Mu, S. Phytic acid-derivative transition metal phosphides encapsulated in N,P-codoped carbon: an efficient and durable hydrogen evolution electrocatalyst in a wide pH range. *Nanoscale* **2017**, *9* (10), 3555−3560.
(37) Pu, Z.; Zhang, C.; Amiinu, I. S.; Li, W.; Wu, L.; Mu, S. General strategy for the synthesis of transition-metal phosphide/n-doped carbon frameworks for hydrogen and oxygen evolution. *ACS Appl. Mater. Interfaces* **2017**, *9* (19), 16187−16193.
(38) Wang, H.; Xu, X.; Ni, B.; Li, H.; Bian, W.; Wang, X. 3D self-assembly of ultrafine molybdenum carbide confined in N-doped carbon nanosheets for efficient hydrogen production. *Nanoscale* **2017**, *9* (41), 15895−15900.
(39) Liu, Y.; Yu, G.; Li, G. D.; Sun, Y.; Asefa, T.; Chen, W.; Zou, X. Coupling Mo_2C with nitrogen-rich nanocarbon leads to efficient hydrogen-evolution electrocatalytic sites. *Angew. Chem., Int. Ed.* **2015**, *54* (37), 10752−7.
(40) Zhou, W. J.; Zhou, Y. C.; Yang, L. J.; Huang, J. L.; Ke, Y. T.; Zhou, K.; Li, L. G.; Chen, S. W. N-doped carbon-coated cobalt nanorod arrays supported on a titanium mesh as highly active electrocatalysts for the hydrogen evolution reaction. *J. Mater. Chem. A* **2015**, *3* (5), 1915−1919.
(41) Cheng, Z.; Fu, Q.; Li, C.; Wang, X.; Gao, J.; Ye, M.; Zhao, Y.; Dong, L.; Luo, H.; Qu, L. Controllable localization of carbon nanotubes on the holey edge of graphene: an efficient oxygen reduction electrocatalyst for Zn−air batteries. *J. Mater. Chem. A* **2016**, *4* (47), 18240−18247.
(42) Jing, S. Y.; Zhang, L. S.; Luo, L.; Lu, J. J.; Yin, S. B.; Shen, P. K.; Tsiakaras, P. N-doped porous molybdenum carbide nanobelts as efficient catalysts for hydrogen evolution reaction. *Appl. Catal., B* **2018**, *224*, 533−540.
(43) Xu, G. R.; Rai, J.; Yao, L.; Xue, Q.; Jiang, J. X.; Zeng, J. H.; Chen, Y.; Lee, J. M. Polyallylamine-functionalized platinum tripods: Enhancement of hydrogen evolution reaction by proton carriers. *ACS Catal.* **2017**, *7* (1), 452−458.
(44) Du, C.; Huang, H.; Wu, Y.; Wu, S.; Song, W. Ultra-efficient electrocatalytic hydrogen evolution at one-step carbonization generated molybdenum carbide nanosheets/N-doped carbon. *Nanoscale* **2016**, *8* (36), 16251−16258.
(45) Politi, J. R.; Vines, F.; Rodriguez, J. A.; Illas, F. Atomic and electronic structure of molybdenum carbide phases: Bulk and low Miller-index surfaces. *Phys. Chem. Chem. Phys.* **2013**, *15* (30), 12617−25.
(46) Kuo, C. H.; Chu, Y. T.; Song, Y. F.; Huang, M. H. Cu_2O nanocrystal-templated growth of Cu_2S nanocages with encapsulated au nanoparticles and in-situ transmission x-ray microscopy study. *Adv. Funct. Mater.* **2011**, *21* (4), 792−797.
(47) Xu, X. Y.; Han, M. R.; Ma, J. Y.; Zhang, C. J.; Li, G. D. Preparation of a nanoporous CuO/Cu composite using a dealloy method for high performance lithium-ion batteries. *RSC Adv.* **2015**, *5* (88), 71760−71764.
(48) Xi, F.; Liu, H.; Li, W.; Zhu, L.; Geng, H.; Quan, L.; Liang, W. Fabricating CuS counter electrode for quantum dots-sensitized solar cells via electro-deposition and sulfurization of Cu_2O. *Electrochim. Acta* **2015**, *178*, 329−335.
(49) Gao, M. R.; Chan, M. K.; Sun, Y. Edge-terminated molybdenum disulfide with a 9.4-Å interlayer spacing for electrochemical hydrogen production. *Nat. Commun.* **2015**, *6*, 7493.
(50) Wu, Y.; Liu, X.; Han, D.; Song, X.; Shi, L.; Song, Y.; Niu, S.; Xie, Y.; Cai, J.; Wu, S.; Kang, J.; Zhou, J.; Chen, Z.; Zheng, X.; Xiao, X.; Wang, G. Electron density modulation of $NiCo_2S_4$ nanowires by nitrogen incorporation for highly efficient hydrogen evolution catalysis. *Nat. Commun.* **2018**, *9* (1), 1425.
(51) Chen, G.-F.; Ma, T. Y.; Liu, Z.-Q.; Li, N.; Su, Y.-Z.; Davey, K.; Qiao, S.-Z. Efficient and stable bifunctional electrocatalysts Ni/Ni_xM_y(M = P, S) for overall water splitting. *Adv. Funct. Mater.* **2016**, *26* (19), 3314−3323.
(52) Ai, L. H.; Su, J. F.; Wang, M.; Jiang, J. Bamboo-structured nitrogen-doped carbon nanotube coencapsulating cobalt and molybdenum carbide nanoparticles: An efficient bifunctional electrocatalyst for overall water splitting. *ACS Sustainable Chem. Eng.* **2018**, *6* (8), 9912−9920.

DOI: 10.1021/acssuschemeng.9b00210
ACS Sustainable Chem. Eng. 2019, 7, 8458−8465

(53) Wei, S. T.; Qi, K.; Jin, Z.; Cao, J. S.; Zheng, W. T.; Chen, H.; Cui, X. Q. One-step synthesis of a self-supported copper phosphide nanobush for overall water splitting. *ACS Omega* **2016**, *1* (6), 1367−1373.
(54) Pu, Z.; Amiinu, I. S.; Liu, X.; Wang, M.; Mu, S. Ultrastable nitrogen-doped carbon encapsulating molybdenum phosphide nanoparticles as highly efficient electrocatalyst for hydrogen generation. *Nanoscale* **2016**, *8* (39), 17256−17261.
(55) Pu, Z.; Wang, M.; Kou, Z.; Amiinu, I. S.; Mu, S. Mo_2C quantum dot embedded chitosan-derived nitrogen-doped carbon for efficient hydrogen evolution in a broad pH range. *Chem. Commun.* **2016**, *52* (86), 12753−12756.
(56) Huang, T.; Chen, Y.; Lee, J.-M. Two-dimensional cobalt/N-doped carbon hybrid structure derived from metal−organic frameworks as efficient electrocatalysts for hydrogen evolution. *ACS Sustainable Chem. Eng.* **2017**, *5* (7), 5646−5650.
(57) Michalsky, R.; Zhang, Y.-J.; Peterson, A. A. Trends in the hydrogen evolution activity of metal carbide catalysts. *ACS Catal.* **2014**, *4* (5), 1274−1278.
(58) Chen, Z.; Song, Y.; Cai, J.; Zheng, X.; Han, D.; Wu, Y.; Zang, Y.; Niu, S.; Liu, Y.; Zhu, J.; Liu, X.; Wang, G. Tailoring the d-band centers enables Co_4N nanosheets to be highly active for hydrogen evolution catalysis. *Angew. Chem., Int. Ed.* **2018**, *57* (18), 5076−5080.
(59) Ji, M.; Niu, S.; Du, Y.; Song, B.; Xu, P. Anion-induced size selection of β-Mo_2C supported on nitrogen-doped carbon nanotubes for electrocatalytic hydrogen evolution. *ACS Sustainable Chem. Eng.* **2018**, *6* (9), 11922−11929.

DOI: 10.1021/acssuschemeng.9b00210
ACS Sustainable Chem. Eng. 2019, 7, 8458−8465